

Enhanced soft x-ray reflectivity of Cr/Sc multilayers by ion-assisted sputter deposition

F. Eriksson

Linköping University
Department of Physics
Thin Film Division
S-58183 Linköping, Sweden
E-mail: freer@ifm.liu.se

G. A. Johansson, MEMBER SPIE

H. M. Hertz, MEMBER SPIE
Royal Institute of Technology
Biomedical and X-Ray Physics
S-10044 Stockholm, Sweden

J. Birch

Linköping University
Department of Physics
Thin Film Division
S-58183 Linköping, Sweden

Abstract. Cr/Sc multilayers have been grown on Si substrates using dc magnetron sputtering. The multilayers are intended as condenser mirrors in a soft x-ray microscope operating at the wavelength 3.374 nm. They were designed for normal reflection of the first and second orders, with multilayer periods of 1.692 and 3.381 nm, and layer thickness ratios of 0.471 and 0.237, respectively. At-wavelength soft-x-ray reflectivity measurements were carried out using a reflectometer with a compact soft-x-ray laser-plasma source. The multilayers were irradiated during growth with Ar ions, varying both in energy (9 to 113 eV) and flux, in order to stimulate the adatom mobility and improve the interface flatness. It was found that to obtain a maximum soft x-ray reflectivity with a low flux (Cr=0.76, Sc=2.5) of Ar ions a rather high energy of 53 eV was required. Such energy also caused intermixing of the layers. By the use of a solenoid surrounding the substrate, the arriving ion-to-metal flux ratio could be increased 10 times and the required ion energy could be decreased. A high flux (Cr=7.1, Sc=23.1) of low-energy (9 eV) Ar ions yielded the most favorable growth condition, limiting the intermixing with a subsistent good surface flatness. © 2002 Society of Photo-Optical Instrumentation Engineers. [DOI: 10.1117/1.1510750]

Subject terms: Cr/Sc; multilayer; reflectivity; ion-assisted sputter deposition; ion energy; ion flux; soft-x-ray microscopy; water window.

Paper 010394 received Nov. 1, 2001; revised manuscript received Apr. 4, 2002; accepted for publication Apr. 9, 2002.

1 Introduction

Multilayer x-ray optics have many useful applications, such as x-ray microscopy,^{1,2} x-ray astronomy,^{3,4} x-ray lithography,⁵ and x-ray microanalysis.⁶ In particular, multilayer mirrors for the water-window region ($\lambda = 2.2$ to 4.4 nm) have an important application as optical elements in microscopy of biological specimens, due to the large absorption contrast between protein and water. In soft x-ray microscopy, using a laser-plasma line source, a multilayer mirror is needed as a condenser to focus the x rays on the specimen.⁷ A primary goal is to maximize the normal-incidence reflectance. To achieve optimum performance it is required that the multilayer period and layer thickness ratio are optimized to add, coherently and in phase, the reflected amplitudes from each interface.

It is known that interfacial roughness leads to a loss of specular reflectivity, which is detrimental for the optical properties.^{8,9} Since the normal-incidence reflectivity R for a given x-ray wavelength λ and reflection order m of a multilayer is greatly influenced by the ratio between the interface roughness σ and the multilayer period Λ according to the Debye-Waller-like factor $\exp[-(2\pi m\sigma/\Lambda)^2]$, the absolute value of the interface roughness becomes more critical at small multilayer periods.^{10,11} For example, model calculations predicts that for a semi-infinite Cr/Sc multilayer, which theoretically is one of the most promising material combinations in the water window, a decrease in interface roughness from 0.5 to 0.3 nm in a multilayer with

period $\Lambda = 1.692$ nm theoretically corresponds to an increase in normal-incidence reflectivity from $R = 2\%$ to $R = 19\%$ for the wavelength $\lambda = 3.374$ nm. Therefore it is important to achieve as smooth and compositionally abrupt interfaces as possible when depositing multilayer x-ray mirrors.

In multilayer mirrors the effects of interface imperfections such as intermixing, interdiffusion, and roughness will be enhanced by the large number of interfaces contributing to the reflectance. There are two main processes in multilayer growth that cause the interface chemical composition profile to broaden, namely, interdiffusion and intermixing. Interdiffusion is thermally activated transport of material across the interface, and intermixing is mixing of the interfaces due to energetic particle bombardment. Both lead to a larger interface concentration gradient, i.e., a larger interface width, and they have the same consequence of reduced specular reflectivity, although they originate from physically different effects. Roughness, on the other hand, may occur even if the interfaces are locally abrupt; the effect is still an increased interface width when the roughness is averaged laterally over the coherence length of the x rays. The influence of roughness on the reflectivity is decreased specular intensity and increased diffuse scattering.

A low substrate temperature and no energetic particle irradiation during growth will minimize interdiffusion and interface mixing. However, such conditions may lead to kinematically limited growth, i.e., the adatoms do not have

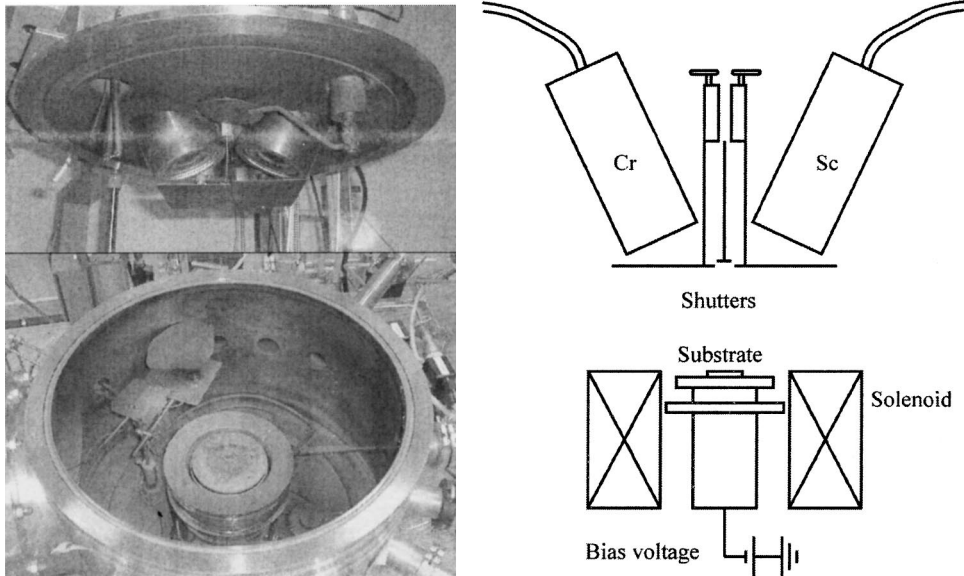


Fig. 1 Dual dc magnetron sputtering system, showing magnetrons, computer-controlled shutters, rotating substrate table, and surrounding solenoid.

high enough surface mobility to find the energetically most favorable sticking position. This leads to increased and accumulated roughness.^{12,13} The exact temperature range where this occurs is not known, but it has been estimated that homologous deposition temperatures (i.e., the ratio between the growth temperature and the melting temperature) $T/T_m < 1/3$ are insufficient to give the required adatom surface mobility to reach the energetically most favorable positions.¹⁴ On the other hand, increasing the substrate temperature, in order to increase the adatom mobility and hence reduce accumulated roughness, may activate bulk diffusion across the interfaces.¹⁵ An apparent increase of the surface temperature, achieved by ion irradiation during growth, will enhance adatom mobility while heating of the bulk multilayer is avoided. Such conditions have been demonstrated to reduce the accumulated roughness,¹⁶ although at the expense of decreased interface abruptness due to intermixing¹⁷ of the interfaces. Post deposition grazing-incidence ion irradiation has also proved to smooth the layers, leading to significantly improved reflectivities.^{18,19} Other effects such as resputtering and defect creation have also been observed.²⁰ It is expected that an increased flux of ions with lower energy would not induce intermixing, while the positive effects of the enhanced adatom mobility remain. A variety of plasma-based deposition techniques exist that might be used for ion-assisted deposition.²¹

The Cr/Sc multilayers in this work were grown at ambient temperature, which corresponds to $T/T_m = 0.14$ and 0.19 for Cr and Sc, respectively, and the multilayers were intentionally irradiated during magnetron sputter deposition with Ar ions of different energies (E) and different ion-to-metal flux ratios (Φ). Ions, extracted from the plasma and accelerated to kinetic energies in the range of 9 to 113 eV through a negative substrate bias, have been utilized in order to stimulate the adatom mobility and improve the interface flatness. The flux of ions was controlled by the use of a solenoid surrounding the substrate, which guides energetic secondary electrons from the target region towards the

vicinity of the substrate, where they increase the plasma density by ionization. By synchronizing both the magnitude and direction of the solenoid current with the deposition from each magnetron, the magnetic field of the solenoid was coupled with the magnetic field of the magnetron used for deposition, and the ion flux density on the substrate could thus be set independently for deposition from each magnetron.

This is an easy way to change and control the plasma growth conditions in a broad region, such that both ion current density and ion energy at the substrate surface can be varied individually for the deposition of the two materials.

2 Experimental Details

The multilayers were deposited using a dual dc magnetron sputtering system (Fig. 1) onto chemically cleaned (10-min ultrasonic cleaning in each of trichlorethylene, acetone, and isopropanol) Si (100) substrates with a native oxide. The rms surface roughness of the identical substrates was 0.3 nm as measured by atomic force microscopy (AFM). The chamber is 500 mm in diameter and 350 mm in height, and the target-to-substrate distance is 120 mm. A background pressure of about 2×10^{-7} Torr (2.67×10^{-5} Pa) is obtained using a turbo molecular pump backed by a rotary vane pump. The two 75-mm-diam magnetrons are placed at the top of the chamber with a tilt angle of 25 deg from the substrate-table normal. The configuration of the magnets in the magnetrons is such that the outer magnetic field lines are positively coupled to each other, guiding secondary electrons away from the cathodes towards the substrate, and thus extending the plasma to the substrate region. Between the magnetrons an electrically isolated μ -metal shield prevents cross-contamination and forces the magnetic field lines to connect beneath the shield closer to the substrate. Ar gas, 99.9997%, was introduced to a working sputtering gas pressure of 3 mTorr (0.4 Pa), as measured with a capacitance manometer.

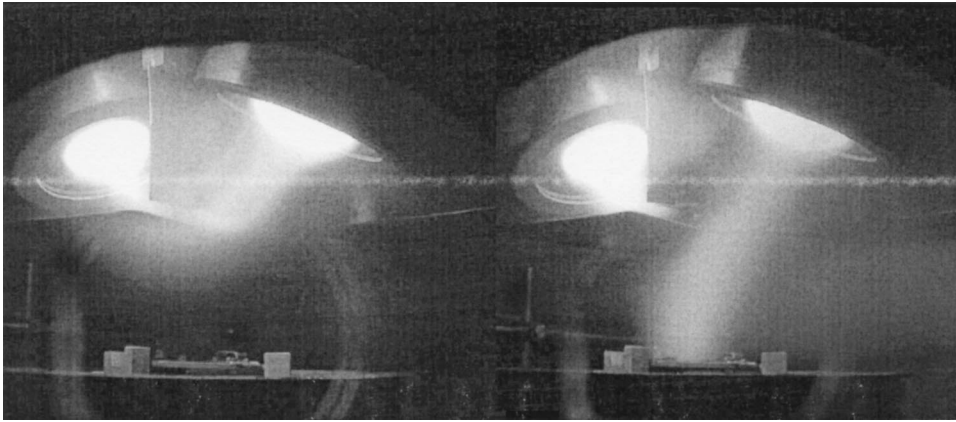


Fig. 2 Photographs of the plasma with a solenoid current of 0 A (on the left) and 5 A (on the right). Secondary electrons ejected from the target are guided towards the substrate, and the plasma density is clearly enhanced in the substrate region when the solenoid is used.

The target discharges were established with constant-current power supplies, and discharge currents (voltages) of 0.060 A (-255 V) and 0.060 A (-280 V) were used for the Sc (99.9%) and Cr (99.94%) targets, respectively. This yielded Sc and Cr deposition rates of about 0.025 and 0.035 nm/s. Both magnetrons were running continuously during the deposition, and the material fluxes to the substrate were regulated by fast-acting computer-controlled shutters located in front of the magnetrons.

The deposition rates were determined by growing two multilayers with different Cr/Sc layer thickness ratios, with known layer deposition times. The multilayer periods were then calculated from the positions of the multilayer peaks in low-angle hard-x-ray reflectivity patterns. This yields an equation system from which the deposition rates can be extracted using Cramer's rule.²²

The substrates ($40 \times 20 \times 0.5$ mm³) were mounted on a substrate table, rotating around the sample normal at a constant rate of 60 rpm, directly in line of sight of both magnetrons, in order to even out irregularities in the sputtered flux. The substrate table was electrically isolated from the system, and a negative bias voltage could be applied to the substrate in order to attract Ar ions from the plasma.

By the use of a solenoid surrounding the substrate, and choosing the direction of the current properly, the magnetic field from either one of the magnetrons could be coupled to the magnetic field of the solenoid. Solenoid currents of 0 and 5 A were utilized in order to study the influence of different fluxes of ions to the substrate. Shown in Fig. 2 are two photographs of the plasma with solenoid currents of 0 and 5 A, respectively. The solenoid was made of capton-insulated Cu wire (2-mm diam) wound about 220 turns on a cylindrical stainless-steel frame with an inner diameter of 125 mm. A detailed characterization of this experimental setup is given in Ref. 23.

Electrical probe measurements were performed to determine the plasma characteristics and the effects of the solenoid. To be able to measure in the electron-current region as well as in the ion-current region, two different probe geometries were used. A Langmuir probe, a 4-mm-long tungsten wire with 0.15-mm radius, was used to determine the floating potential and the plasma potential. The kinetic

energy of the Ar ions is then simply obtained as the difference between the plasma potential and the applied bias voltage, since the mean free path of the Ar ions (several centimeters) is much larger than the dark sheath above the substrate (less than a millimeter). For the ion current density measurements a flat probe of stainless steel, 15 mm in diameter, was used. The probe was surrounded by a flat stainless-steel shield with the same potential as the probe, in order to prevent edge effects from influencing the effective collecting probe surface. Data collection was performed by sweeping the bias voltage and simultaneously measuring the probe current. From these data the ion-to-metal flux ratios Φ could be determined. Both probes were positioned on the substrate holder at the focal point of the magnetrons.

Nanostructural properties of the multilayer structures were obtained from hard-x-ray low-angle reflectivity measurements, using a Philips powder diffractometer with a copper anode source (Cu $K\alpha$, $\lambda = 1.54$ Å), operating at 0.8 kW and with an accuracy of 0.015 deg in 2θ . A counting time of 2.5 s was used at each 2θ increment of 0.005 deg. The Cu $K\beta$ radiation was attenuated by a Ni filter between the source and the sample. Directly after the x-ray source a 0.25-deg divergence slit and a 2-mm-wide brass mask were used to collimate the beam and to limit the size of the x-ray beam on the sample. In front of the detector a 0.1-mm antiscatter slit and a 0.25-deg divergence slit followed by a curved Ge crystal monochromator were used. The diffractometer had decoupled detector (2θ) and sample (ω) axes so that coupled ω - 2θ scans as well as ω -rocking curves could be performed. The intensity was detected with a proportional Xe-gas-filled detector.

Specular hard x-ray reflectivity measurements from 0.7 to 20 deg in 2θ were performed on all samples. From these the multilayer periods were calculated from the position of the Bragg reflections. Individual layer thicknesses and interface widths were determined by fitting model calculations of the specular reflectivity to the experimental data using the Wingixa software²⁴ from Philips. Nonspecular transverse ω -rocking scans for constant 2θ values, corresponding to the first Bragg peak reflection of the investigated multilayers, were also performed. These scans reveal

how much of the x-rays is specularly reflected and how much diffusively scattered, and hence gives qualitative information about the interface roughness.

The near-normal at-wavelength reflectivity of the multilayers was investigated using a soft-x-ray reflectometer operating at the same wavelength as the microscope for which the mirrors are designed.^{7,25} The reflectometer is based on a high-brightness line-emitting laser-plasma source utilizing an ethanol liquid-jet target emitting mainly $\lambda = 3.374$ nm, corresponding to the carbon VI line. By using a multilayer with known absolute reflectivity as a calibration standard, absolute reflectivity up to 85-deg grazing incidence angle was measured. The detector system consists of two soft-x-ray photodiodes, one for measuring the reflected x rays and the other for monitoring the source intensity. The reference sample, a Cr/Sc multilayer with 100 bilayers and a period of 3.468 nm, was measured at the Calibration and Standards Beamline 6.3.2 at the Advanced Light Source. The reflectivity of the reference sample was 10% at a grazing angle of 29.3 deg and 0.4% at 77.8 deg for the first- and the second-order reflectivity, respectively. By performing comparative measurements with the reference multilayer it is possible to measure the absolute reflectivity of other samples.

To calculate the optimal design of the multilayers (i.e., the period, the layer thickness ratio, and the total number of bilayers for maximal reflectivity), the IMD code²⁶ was utilized. This yielded a multilayer period of $\Lambda = 1.692$ nm and a layer thickness ratio of $\Gamma = d_{Cr}/\Lambda = 0.471$ for multilayers designed for the first-order normal reflection, and $\Lambda = 3.381$ nm and $\Gamma = 0.237$ for the second order. Using the same code, it was predicted that 90% of the expected theoretical normal-incidence reflectivities from semi-infinite multilayer stacks (35% for $\Lambda = 1.692$ nm and 23% for $\Lambda = 3.381$ nm) should be achieved with about 300 bilayers of $\Lambda = 1.692$ nm and 270 bilayers of $\Lambda = 3.381$ nm. However, in order to reflect the x rays below 85 deg, which is the upper limit of the reflectometer, the multilayer period had to be slightly larger, about $\Lambda = 1.75$ and 3.5 nm for mirrors designed for the first- and second-order reflection, respectively.

3 Results and Discussion

From electrical probe measurements it was found that the ion-to-metal flux ratios were $\Phi_{Cr} = 0.76$ and $\Phi_{Sc} = 2.5$ without the solenoid. When changing the solenoid current from 0 to 5 A, the ratios increased by about 10 times for both Cr and Sc, to $\Phi_{Cr} = 7.1$ and $\Phi_{Sc} = 23.1$, respectively. The plasma potential did not vary between Cr and Sc deposition, but it decreased by 14 V, from 8.0 to -6.1 V, when the solenoid current was increased. Thus, the energy of the ions, $E_{ion} = e|V_p - V_s|$ (assuming univalent ions), attracted by the substrate is 8.0 eV higher and 6.1 eV lower than that indicated by the substrate bias potential when the coil is off and on, respectively. The floating potentials V_f were the same for both Cr and Sc and were determined to be $V_f = -15$ and -4 V with and without the use of the solenoid. This shows that considerably more secondary electrons are guided towards the substrate when the solenoid is coupling to a magnetron, and consequently more Ar is ionized in the

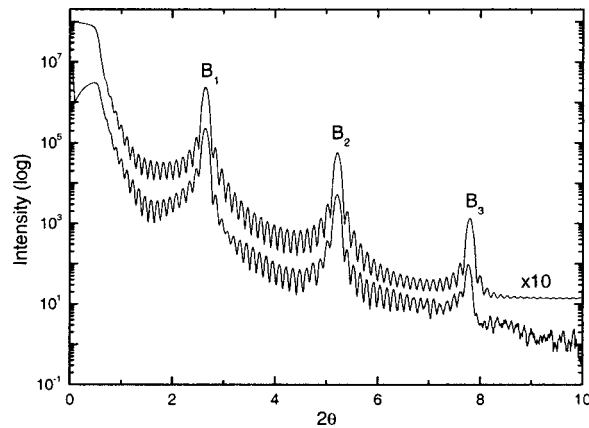


Fig. 3 Hard x-ray ($\text{Cu K}\alpha$) reflectivity measurement of a multilayer containing 20 bilayers optimized for the second-order reflection of $\lambda = 3.374$ nm, together with a simulation. The simulated intensity is increased 10 times for clarity.

vicinity of the substrate. This in turn means that a lower bias voltage is required to attract a larger number of Ar ions from the plasma, permitting ion-stimulated adatom mobility using very low-energy ions to reduce intermixing effects.

To study the effects of different deposition ion energies for solenoid currents of 0 and 5 A, i.e., using low ($\Phi_{Cr} = 0.76$, $\Phi_{Sc} = 2.5$) and high ($\Phi_{Cr} = 7.1$, $\Phi_{Sc} = 23.1$) fluxes of Ar ions at the sample, hard x-ray $\text{Cu K}\alpha$ reflectivity measurements were performed on multilayers grown with different ion energies.

Figure 3 shows a hard x-ray reflectivity curve together with a simulation. The multilayer, which was designed for the second-order reflection of $\lambda = 3.374$ nm, contains 20 bilayers and was deposited using a high Ar ion flux with an energy of 24 eV.

The three major peaks (marked B_1 , B_2 , and B_3 in the figure), at $2\theta_1 = 2.65$ deg, $2\theta_2 = 5.22$ deg, and $2\theta_3 = 7.79$ deg, are the first-, second-, and third-order multilayer Bragg reflections, respectively, and the positions correspond to a multilayer period of $\Lambda = 3.410$ nm. Between the Bragg reflections, and all the way up to the third reflection order, very distinct and sharp Kiessig fringes are visible. These oscillations are due to the interference of x rays that have been reflected from different interfaces. Each peak in the Fourier domain is associated with the distance between two interfaces. The number of Kiessig fringes is thus related to the number of bilayers in the multilayer. These regular distances will become irregular if layer thickness variations exist, and thus their highly regular presence is an evidence of a very high layer uniformity.

The simulation corresponds very well with the measurement. The discrepancy below the critical angle, $2\theta_C = 0.53$ deg, is due to the finite size of the sample, which could not be included in the simulation. At first the x rays are passing straight into the detector, and as the angle increases the x rays start to be totally reflected from the sample. Because of the limited size of the sample (20 mm), some of the x rays will pass by the sample and hence not reach the detector, resulting in an intensity loss. As the angle is further increased, more of the x-ray beam illumi-

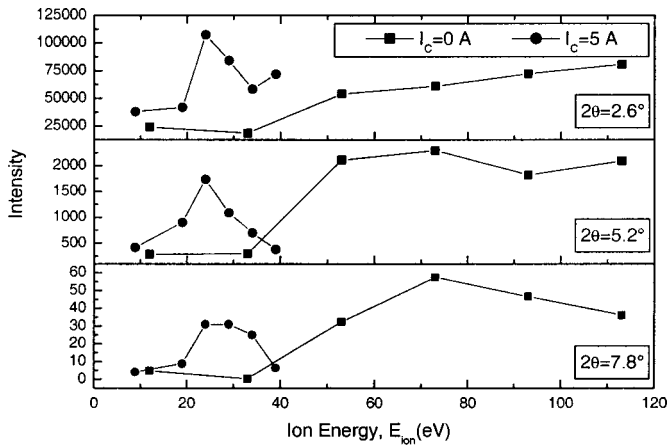


Fig. 4 Hard x-ray specular reflectivity of the first three orders of multilayer Bragg reflections as a function of the ion energy for low and high ion fluxes, i.e., solenoid currents $I_C=0$ and 5 A, respectively.

notes the sample and the intensity increases. Above the critical angle all x rays are incident on the sample.

The simulation yielded individual layer thicknesses of $d_{Sc}=2.766$ nm and $d_{Cr}=0.641$ nm, i.e., a multilayer period of $\Lambda=3.407$ nm and a layer thickness ratio of $\Gamma=0.188$. This multilayer period is in very good agreement with the one calculated from the position of the Bragg peaks. The average interface width of the multilayer was determined to be 0.962 nm. The notation interface width combines two physically different aspects of an interface, the local chemical composition profile width (a result of atomic bulk displacement processes such as interdiffusion and intermixing), and interfacial roughness (related to surface displacement processes). A chromium oxide layer was added in the simulation in order to fit the intensity of the Kiessig fringes between the Bragg reflections.

In Fig. 4 the intensities of the first three Bragg reflections ($2\theta_1=2.6$ deg, $2\theta_2=5.2$ deg, and $2\theta_3=7.8$ deg) are plotted as a function of the ion energy. For low Φ , the first Bragg peak increases for all ion energies. However, the second and third Bragg peaks, which are more roughness-sensitive, decrease for energies above 73 eV, which indicates that an optimal ion energy exists for obtaining high reflectivity of the mirrors. For the multilayers deposited with a large Φ an optimal ion energy of 24 eV is clearly evident.

Thus, depositing multilayers with varying ion energies resulted in peaked behavior of the x-ray reflectivities for both low and high fluxes of Ar ions. Below the maxima the increasing reflectivities are due to decreasing interface roughness, which can be attributed to increased surface mobilities, caused by the attracted Ar ions, during the whole deposition of each layer. An increase in surface mobility allows the deposited adatoms to move around on the surface and find positions with a local energy minimum, which in turn means a position that smooths the surface. For a continuing increase in ion energy beyond the reflectivity maxima at 24 and 73 eV, the observed decreases are due to the knock-on effects of the increasing energy of the Ar ion bombardment, resulting in intermixing of the layer materials. Similar effects have been observed in both amorphous

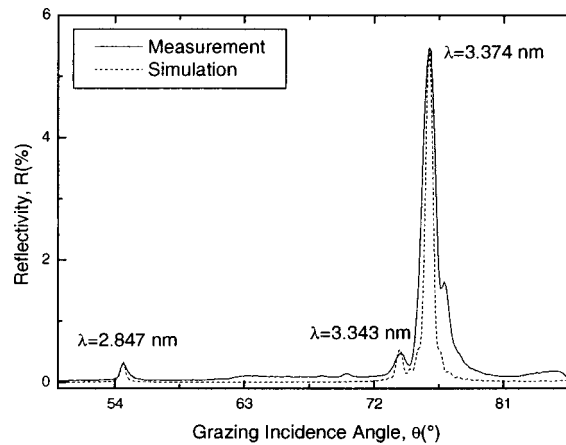


Fig. 5 Soft x-ray reflectivity measurement of a multilayer consisting of 400 bilayers optimized for the first-order reflection of $\lambda=3.374$ nm, together with a simulation. Since the soft x-ray source consists of an ethanol target, the spectrum contains several wavelengths, which are also detected.

multilayers¹⁶ and single-crystal superlattices.²⁷ Another possible explanation of the decreased reflectivities may be an increasing *waviness* of the layers caused by nucleation of islands. Such nucleation may occur if nonwetting conditions apply and if the mobility of adatoms is high enough. However, increased waviness would also mean increased interlayer roughness correlation, leading to increased broadening of rocking scans over the Bragg peaks.

Rocking scans were performed (not shown) for three different ion energies (low, optimal, and high) for each of the two ion fluxes. Decreased rocking-curve widths with increasing ion energy for both ion fluxes were observed, showing that the interlayer roughness correlation decreased, which thus excludes increased waviness as the cause of decreased reflectivity at higher energies.

Figure 5 shows an at-wavelength ($\lambda=3.374$ nm) soft x-ray reflectivity measurement with the highest obtained reflectivity, $R=5.47\%$ at a grazing incidence angle of 76 deg, for a multilayer deposited with high ion flux and an ion energy of 24 eV. Since the laser-plasma source is using an ethanol target, several deexcitation processes take place and give rise to other soft x-ray wavelengths. These wavelengths are also reflected by the multilayer and appear in the measured spectrum. Included in the graph is an IMD simulation of the wavelengths $\lambda=2.847$, 3.343, and 3.374 nm, all corresponding to carbon deexcitations. To obtain a good fit, first the peak position was obtained by varying the multilayer period for the fixed wavelength $\lambda=3.374$ nm. Thereafter the simulated reflectivity was decreased to the measured value by increasing the interface width. This resulted in a multilayer period of $\Lambda=1.746$ nm and an average interface width of 0.425 nm. In the simulations the layer thickness ratio was fixed at the nominal value, $\Gamma=0.471$, and since the first-order reflectivity does not vary much with Γ , a small error in Γ should not significantly influence the simulation. The peak broadening that can be seen is because of a small continuous drift of the period in the multilayer due to target erosion effects. Based on the peak width, the drift is estimated, using the IMD simulation software, to about 1.5×10^{-5} nm per bilayer thickness.

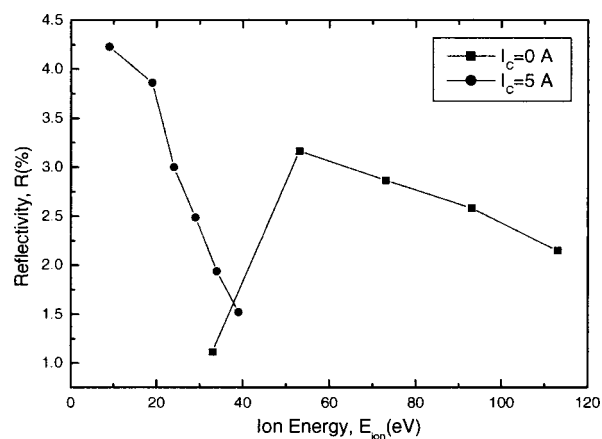


Fig. 6 Soft x-ray reflectivity of the first-order reflection of $\lambda = 3.374$ nm as a function of the ion energy for solenoid currents of $I_c = 0$ and 5 A.

Figure 6 shows the soft x-ray reflectivities of multilayers grown with different ion energies for low and high fluxes of ions, i.e., $I_c = 0$ and 5 A, respectively. The multilayers are designed to have the second-order reflection of $\lambda = 3.374$ nm at near-normal incidence, and this figure shows the first-order reflection, which appears at a grazing incidence angle close to 30 deg.

Again the reflectivity shows peaked behavior for the case of low Ar flux, but now with a maximum at an ion energy of about 53 eV. The reflectivity for the high Ar flux has its highest value at 9 eV, corresponding to growth with the sample at floating potential. Although this is not confirmed to be an optimum, it is not expected that a lower bias voltage, which causes predominantly electron bombardment instead of ion bombardment, will improve the reflectivity further. A substrate bias potential above the floating potential will quickly produce electron currents up to several orders of magnitude higher than the ion currents, thus causing resistive heating of the sample with a possible increase of the bulk interdiffusion as a consequence.

The reason for this behavior follows the same arguments as given above for the hard x-ray reflectivities. The increase in reflectivity is due to the decreased roughness, and then beyond a certain ion energy the intermixing takes over and the reflectivity decreases. Notable is the much higher maximal absolute reflectivity that occurs already for 9-eV ions under high-flux conditions.

As can be seen from the Figs. 4 and 6, the maximum reflectivities does not occur at the same ion energies for hard x rays and soft x rays. For the high ion flux, the soft x-ray maximum occurs at a low ion energy, about 9 eV, versus 24 eV in the case of hard x-rays. For low ion flux, the soft and hard x-ray reflectivity maxima appear at about 53 and 73 eV, respectively.

The difference is due to the fact that the reflectivity of hard x rays, which have a wavelength on the atomic scale, is sensitive to roughness down to that scale, sometimes referred to as *jaggedness*.²⁸ Soft x rays, on the other hand, have a wavelength that is 20 times longer, and the soft x-ray reflectivity is thus less sensitive to roughness on the atomic scale, but very sensitive to lower spatial frequencies, sometimes called *waviness*. Atomic-scale roughness is

sensed by soft x-ray reflectivity as interdiffusion, i.e., no diffuse scattering is produced. This is also clear on comparing the x-ray coherence lengths parallel to the interfaces for the two measurement setups. These are >1000 nm and <25 nm for soft and hard x-ray reflectivities, respectively.²⁹

At low ion energies, i.e., for low mobility of the adatoms, the kinematically limited growth will produce asperities, with relatively loosely bound top atoms, on the surface. This leads to an increased and accumulated roughness as the growth of the multilayer proceeds. Both the hard and soft x-ray reflectivities will be low. As the ion energy increases, these loosely bound atoms will move around on the surface and find positions where they minimize the total energy, which are positions that smooth the surface. The lower height of the asperities implies a decreased accumulated roughness and lower amplitude of the waviness. However, the atomic-scale roughness may still be of the same order. Such a roughness evolution has been demonstrated in, e.g., Ag/Fe multilayers.³⁰ Thus, the soft x-ray reflectivity will increase while the hard x-ray reflectivity remains low. A further increase in ion energy now experience a flat but intermixed interface and the reflectivity goes down, and at the same time diffuse scattering is eliminated. The hard x rays, on the other hand, experience a decreased atomic-scale roughness, and the reflectivity goes up. Higher ion energies causes intermixing on the atomic level, now eliminating the diffuse scattering also for hard x-rays, and both hard and soft x-ray reflectivities go down.

Thus, the reason for the different positions of the maxima using the two x-ray wavelengths must be that as the ion energy is increased, first the waviness is reduced, resulting in an optimum for soft x-rays, and after a further increase of the ion energy the jaggedness is eliminated. During the whole course of increasing the ion energy the intermixing increases.

Although hard x-ray reflectivity is a very useful tool to obtain the multilayer period, individual layer thicknesses, and interface widths, it can be concluded that the optimal deposition parameters must be determined using the actual wavelength for which the multilayer mirror is intended.

4 Concluding Remarks

As can be seen in Fig. 6, the reflectivity of the multilayer deposited with a high-flux, low-energy Ar bombardment is substantially higher than that of a multilayer deposited with a relatively low-flux, high-energy bombardment. From the discussion above it is clear that this improvement is because of a reduced intermixing for low-energy bombardment and remaining high surface mobility, owing to the high ion flux, that minimizes the waviness.

From the hard x-ray peak reflectivity data we conclude that a higher ion energy is required to reduce the jaggedness than to reduce the waviness. From the above we can conclude that a high flux (7.1 and 23.1 ions per metal atom for Cr and Sc, respectively) of low-energy (9 eV) Ar ions minimizes the intermixing, while the smoothing effect is still present. These conditions cannot be obtained in ordinary magnetron sputtering setups, which typically yield a low density of high-energy ions. These findings are also important in other areas of thin-film deposition, such as

epitaxy and deposition on semiconductor surfaces or on temperature-sensitive surfaces, where creation of surface defects must be avoided or the bulk temperature must be kept at a minimum.

Acknowledgments

The authors are grateful to E. M. Gullikson for his help and support in facilitating the soft x-ray absolute reflectivity measurements, made at the Calibration and Standards Beamline 6.3.2 at the ALS, of the multilayer mirror that was used as a calibration standard.

References

1. M. Berglund, L. Rymell, M. Peuker, T. Wilhein, and H. M. Hertz, "Compact water-window transmission x-ray microscopy," *J. Microsc.* **197**, 268–273 (2000).
2. H. M. Hertz, M. Berglund, G. A. Johansson, M. Peuker, T. Wilhein, and H. Brismar, "Compact water-window x-ray microscopy with a droplet laser-plasma source," in *X-Ray Microscopy*, W. Mayer-Ilse, T. Warwick, and D. Attwood, Eds., p. 721, American Inst. of Physics (2000).
3. A. B. C. Walker, Jr., T. W. Barbee, Jr., R. B. Hoover, and J. F. Lindblom, "Soft x-ray images of the solar corona with a normal-incidence cassegrain multilayer telescope," *Science* **241**, 1781–1787 (1988).
4. E. Spiller, D. G. Stearns, and M. Krumrey, "Multilayer x-ray mirrors: interfacial roughness; scattering, and image quality," *J. Appl. Phys.* **74**, 107–118 (1993).
5. D. G. Stearns, R. S. Rosen, and S. P. Vernon, "Multilayer mirror technology for soft x-ray projection lithography," *Appl. Opt.* **32**, 6952–6960 (1993).
6. A. Grudsky and A. Rudnev, "New possibilities in x-ray microanalysis of nitrogen and oxygen with the application of special types of multilayers," in *Optics and Microanalysis 1992, Proc. Thirteenth Int. Congress*, pp. 95–98, IOP, Bristol, UK (1993).
7. H. M. Hertz, L. Rymell, M. Berglund, G. A. Johansson, T. Wilhein, Y. Platonov, and D. Broadway, "Normal-incidence condenser mirror arrangement for compact water-window x-ray microscopy," in *X-Ray Optics, Instruments, and Missions II, SPIE Annual Meeting, Proc. SPIE* **3766**, 247 (1999).
8. D. E. Savage, J. Kleiner, N. Schimke, Y.-H. Phang, T. Jankowski, J. Jacobs, R. Kariotis, and M. G. Lagally, "Determination of roughness correlations in multilayer films for x-ray mirrors," *J. Appl. Phys.* **69**, 1411–1424 (1991).
9. D. L. Windt, R. Hull, and W. K. Waskiewicz, "Interface imperfections in metal/Si multilayers," *J. Appl. Phys.* **71**, 2675–2678 (1992).
10. C. C. Walton, G. Thomas, and J. B. Kortright, "X-ray optical multilayers: microstructure limits on reflectivity at ultra-short periods," *Acta Mater.* **46**, 3767–3775 (1998).
11. S. S. Andreev, S. R. Müller, Yu. Ya. Platonov, N. I. Polushkin, N. N. Salashchenko, F. Schäfers, S. I. Shinkarev, D. M. Simanovsky, and S. Yu. Zuev, "Small d -spacing multilayer structures for the photon energy range $E > 0.3$ keV," in *Superintense Laser Fields, Proc. SPIE* **1800**, 195–208 (1991).
12. E. E. Fullerton, I. K. Schuller, and Y. Bruynseraede, "Quantitative x-ray diffraction from superlattices," *MRS Bull.* **XVII**(12), 33–38 (1992).
13. H.-J. Voorma, E. Louis, N. B. Koster, and F. Bijkerk, "Temperature induced diffusion in Mo/Si multilayer mirrors," *J. Appl. Phys.* **83**(9), 4700–4708 (1998).
14. C. P. Flynn, "Constraints on the growth of metallic superlattices," *J. Phys. F: Met. Phys.* **18**, L195 (1988).
15. J. Birch, Y. Yamamoto, L. Hultman, G. Radnoczi, J.-E. Sundgren, and L. R. Wallenberg, "Growth and structural characterization of single-crystal (001) oriented Mo-V superlattices," *Vacuum* **41**, 1231–1233 (1990).
16. K. Järrendahl, J. Birch, L. Hultman, L. R. Wallenberg, G. Radnoczi, H. Arwin, and J.-E. Sundgren, "Growth of Ge/Si amorphous superlattices by dual-target dc magnetron sputtering," *Mater. Res. Soc. Symp. Proc.* **258**, 571–575 (1992).
17. S. P. Vernon, D. G. Stearns, and R. S. Rosen, "Ion-assisted sputter deposition of molybdenum-silicon multilayers," *Appl. Opt.* **32**(34), 6969–6974 (1993).
18. E. J. Puik, M. J. van der Wiel, H. Zeijlemaker, and J. Verhoeven, "Ion etching of thin W layers: enhanced reflectivity of W-C multilayer coatings," *Appl. Surf. Sci.* **47**, 63–76 (1991).
19. E. Spiller, "Smoothing of multilayer x-ray mirrors by ion polishing," *Appl. Phys. Lett.* **54**, 2293–2295 (1989).
20. G. Håkansson, J. Birch, L. Hultman, I. P. Ivanov, J.-E. Sundgren, and L. R. Wallenberg, "Ion irradiation effects during growth of Mo/V(001) superlattices by dual-target magnetron sputtering," *J. Cryst. Growth* **121**, 399–412 (1992).
21. J. M. Schneider, S. Rohde, W. D. Sproul, and A. Matthews, "Recent developments in plasma assisted physical vapour deposition," *J. Phys. D* **33**, 173–186 (2000).
22. E. B. Svedberg, J. Birch, C. N. L. Edvardsson and J.-E. Sundgren, "Real time measurements of surface growth evolution in magnetron sputtered single crystal Mo/V superlattices using *in situ* RHEED analysis," *Surf. Sci.* **431**, 16–25 (1999).
23. C. Engström, T. Berling, J. Birch, L. Hultman, I. P. Ivanov, S. R. Kirkpatrick, and S. Rohde, "Design, plasma studies, and ion assisted thin film growth in an unbalanced dual target magnetron sputtering system with a solenoid," *Vacuum* **56**, 107–113 (2000).
24. D. K. G. de Boer, "Glancing-incidence x-ray fluorescence of layered materials," *Phys. Rev. B* **44**, 498 (1991).
25. G. A. Johansson, M. Berglund, F. Eriksson, J. Birch, and H. M. Hertz, "Compact soft x-ray reflectometer based on a line-emitting laser-plasma source," *Rev. Sci. Instrum.* **72**, 58–62 (2001).
26. D. L. Windt, "IMD: software for modeling the optical properties of multilayer films," *Comput. Phys.* **12**, 360–370 (1998).
27. E. B. Svedberg, J. Birch, I. Ivanov, E. P. Münger, and J.-E. Sundgren, "Asymmetric interface broadening in epitaxial Mo/W(001) superlattices grown by magnetron sputtering," *J. Vac. Sci. Technol. A* **16**, 633–638 (1998).
28. D. K. G. Boer and A. J. G. Leenaers, "Probing interface roughness by x-ray scattering," *Physica B* **221**, 18–26 (1996).
29. J. Birch, F. Eriksson, G. Johansson, and H. Hertz, "Recent advances in ion-assisted growth of Cr/Sc multilayer x-ray mirrors for the water window," *Vacuum* (2002).
30. G. Gladyszewski, C. Jaouen, A. Declémy, J. C. Girard, and P. Guerin, "Ion-assisted deposition of Ag(001)/Fe(001) multilayers: interface roughness," *Thin Solid Films* **319**, 44–48 (1998).

Biographies and photographs of the authors not available.